

# Predicting integers from continuous parameters

Bas Maat<sup>◦</sup> and Peter Bloem<sup>◦</sup>

Learning & Reasoning Group  
Vrije Universiteit Amsterdam  
research@basmaat.com, p.bloem@vu.nl

**Abstract.** We study the problem of predicting numeric labels that are constrained to the integers or to a subrange of the integers. For example, the number of up-votes on social media posts, or the number of bicycles available at a public rental station. While it is possible to model these as continuous values, and to apply traditional regression, this approach changes the underlying distribution on the labels from discrete to continuous. Discrete distributions have certain benefits, which leads us to the question whether such integer labels can be modeled directly by a discrete distribution, whose parameters are predicted from the features of a given instance. Moreover, we focus on the use case of output distributions of neural networks, which adds the requirement that the *parameters* of the distribution be continuous so that backpropagation and gradient descent may be used to learn the weights of the network. We investigate several options for such distributions, some existing and some novel, and test them on a range of tasks, including tabular learning, sequential prediction and image generation. We find that overall the best performance comes from two distributions: *Bitwise*, which represents the target integer in bits and places a Bernoulli distribution on each, and a discrete analogue of the Laplace distribution, which uses a distribution with exponentially decaying tails around a continuous mean.

**Keywords:** Regression · Integer regression · loss functions

## 1 Introduction

Consider—as a running example—the problem of modeling MIDI music in a neural network: a sequence of events that captures a musician playing an instrument. The recording does not consist of the raw sound, as in an MP3 file, but of which note was played when, with what intensity and for how long. A model that predicts the next note given what has come before, must produce several pieces of information. Chiefly, which note will be played, and how long the note will be held.

The first part is expressed in MIDI as a choice from 128 discrete options. For this choice, a categorical distribution over all notes is well suited. A neural

---

<sup>◦</sup> Shared first authors.

network can easily produce such a distribution by generating parameters in a 128-element probability vector  $\mathbf{p}$ , using a softmax activation. We then train the neural network to minimize the negative log-probability  $-\log p_i$ , where  $i$  is the note that was actually played.

The second part, how long to hold the note, is a length of time, expressed in the MIDI standard as a discrete number of *ticks* (with one tick commonly corresponding to about 5ms). A natural approach is to model the prediction of an amount of time as a *regression problem*: we treat the number of ticks as a continuous value, ignoring its discrete nature, and we take the mean squared error as a loss function. This loss may be interpreted as the negative log-probability density under a normal distribution for which the neural network produces the mean, so in some sense we are taking the same approach for the note as for the ticks: the neural network parametrizes a probability distribution and we minimize the negative logarithm of the probability or probability density of the true labels.

A problem arises, however, if we want to combine the negative log probabilities of these predictions into a single loss value. The negative log probability under the categorical distribution has a natural interpretation: it is the number of bits that we would use if we represented the target value, using a code derived from the probability distribution [20, Section 3.2]. Such values are well-behaved: they have a minimum value of zero and if we have multiple labels, they can be summed together for a natural loss over all labels.

For the ticks, however, we are taking the negative log-probability *density*. This is not a value in bits, and it's a value that is much less well-behaved: if we compute the full probability density (rather than just the squared distance) it can be negative, and summing it with the negative log-probability from a discrete distribution—like the one we get over the notes—has no natural interpretation. This means that when we use both distributions in a loss function, we must choose ourselves how to balance the two values.

Which brings us to our research question. For a task which includes integer labels, can we perform regression *without* re-interpreting the labels as continuous values? That is, can we devise a distribution on the integers, possibly constrained to a given range, which is suitable for the purposes of regression?

This is not a novel problem, and some approaches exist. However, we will focus on regression models that are optimized by backpropagation and gradient descent: i.e. *neural networks*. This gives us three additional requirements:

1. While the sample space of the distribution (the integers) is *discrete*, its parameters should be *continuous*. This will allow us to define a gradient of the negative log-probability with respect to the parameters, which we can then backpropagate through whatever mechanism produced the parameters.
2. The gradient should be *well-behaved*. It should, ideally, be defined everywhere, and not come too near 0 at any point in the parameter space, or have too many discontinuities.
3. The distribution should be able to “peak” around an arbitrary point. That is, if we make a prediction  $x$  about which we are very certain, the we should

be able to set the parameters in such a way that almost all probability is assigned to  $x$ .<sup>1</sup>

We identify three existing candidates to be used as baselines and introduce three more novel approaches.

In order, these are:

**Discrete Weibull** A discrete analogue of the Weibull distribution.

**Discretized Normal** The normal distribution, discretized by assigning the probability mass on the interval  $[x - \frac{1}{2}, x + \frac{1}{2})$  to the integer  $x$ .

**Discretized Laplace**<sup>2</sup> The Laplace distribution, discretized in the same way.

**Dalap** Short for *discrete analogue to the Laplace distribution*. Takes the form  $p(n) \propto \gamma^{|n-\mu|}$ . This distribution was introduced with a discrete parameter  $\mu$  in [23]. We extend this to a continuous parameter, and derive the partition function.

**Danorm** Short for *discrete analogue to the Normal distribution*. Takes the form  $p(n) \propto \gamma^{(n-\mu)^2}$ . Introduced in a different form in [24]. We use the form above, by analogy with Dalap, and approximate the partition function.

**Bitwise** This distribution is based on the common idea of representing an integer as a bitstring, in sign-magnitude representation, and having a model produce a Bernoulli distribution for each bit. While this representation is common in neural networks, we have not found references that interpret the resulting model as a distribution on the integers.

We study these distributions in three settings. First, we define three tabular regression tasks with integer labels. These are based on the number of bicycles available at public rental stations, the number of upvotes on content in a social media setting and the net migration between countries. Next, we test the models in a sequential prediction setting. Specifically, the the MIDI music problem that we used to motivate our research question at the start of this section. We isolate the issue of predicting the ticks on the following note, given the sequence of events that came before. Finally, we show a proof-of-concept for integer prediction in the image generation domain. We train an autoregressive pixel model on images, treating each channel of each pixel as an integer prediction problem restricted to the range  $[0, 255]$ .

Our findings are that Dalap or Bitwise outperform the existing distributions in most cases, when performance is measured in negative log-probability. When measured in (root) mean squared error, Danorm performs best, sometimes slightly outperforming a plain squared error loss. However, due to the very rapidly decaying tails, the negative log-probability of Danorm is much higher than that of the other distributions.

In all tabular data, relaxing the problem to continuous target labels leads to a better RMSE score than any of the discrete distributions, suggesting that in most

---

<sup>1</sup> This rules out, for example, the Poisson distribution. Its parameter  $\lambda$  is continuous and its sample space discrete, but the probability mass cannot be made arbitrarily concentrated on a given integer.

<sup>2</sup> Code is available at <https://github.com/pbloem/contin>

settings, that is likely still the preferred approach. However, when a discrete distribution is required, Bitwise, Dalap and Danorm are likely the best options.

## 2 Related Work

We briefly discuss the large variety of models for count data (i.e. those supported on  $\mathbb{N}$ ) and for integer data (supported on  $\mathbb{Z}$ ). Most of these do not fit our requirements outlined in the introduction. Others have had to be excluded to keep the scope of the present research manageable.

### 2.1 Count models

A subset of regression on integer-valued labels is that of modeling *count data*, where the labels are restricted to the non-negative or positive integers and usually represent counts of items or events. This problem is well-studied and is often tackled with Poisson or negative binomial distributions [11,22].

While our approach shares a lot with this existing line of research, the focus on neural network modeling changes the problem in some significant ways. First, we are not interested in closed-form solutions, or convergent optimization for the optimal parameters, since these properties are not available for the weights of the neural network in any case. Second, in our setting the parameters of the distribution are required to be continuous, so that a gradient can be defined for them. And, finally, we are only interested in conditional modeling: predicting integer labels given some features or other conditioning information, rather than fitting a single distribution to a whole population.

*Poisson-based* A very common family of approach is built on the Poisson distribution. Since this distribution has only one parameter, the mean and variance must be related. In fact in the Poisson distribution, they are equal. This is referred to as equidispersion. Various extensions have been proposed [9] to allow for overdispersion (a variance higher than the mean) and underdispersion (a variance lower than the mean). However, this still puts a lower or upper bound on the variance that depends on the chosen mean. For our purposes, we require a distribution where the variance can be set independently from the mean, as it is in, for example, the normal distribution. Ideally, the distribution can be parameterized directly in terms of the required location and dispersion. Later models in this family offer great flexibility in the dispersion [35], but this often comes at the cost of difficult to estimate probabilities. For these reasons we consider this family as a whole out of scope.

*Discrete Weibull* One prominent example of a discrete distribution with continuous parameters, is the *Discrete Weibull distribution* [28,13,16]. We include this as a baseline and describe it briefly in the next section. Generalizations include the exponentiated discrete Weibull distribution [30], which can take bimodal ("bathtub") shapes as well as unimodal. For our purposes, this is not required behavior, so we consider generalizations out of scope.

*Geometric distributions* As the tails of Dalap follow a geometric progression, it is related to the geometric distribution. Some other discrete generalizations of the geometric distribution exist. One example is [18], which allows the mode to take values other than 0. However, in this distribution, the mean is not a straightforward function of the parameters, and the mean and dispersion are not independent, which are important properties for our use case.

*Others* There are other discrete distributions, which due to their shape, we did not consider promising candidates. These include the discrete Lindley distribution [19], the discrete Rayleigh distribution [33] and the discrete Burr-Hatke distribution [15]. In general these models are likely to show overdispersion in a neural network setting. That is, the data distribution (conditioned on a particular set of feature-values) is likely to form a low-variance, high peaked distribution around a single value, which the distribution cannot represent.

## 2.2 Integer models

The broader problem of *integer regression*, where the target label is a discrete, but potentially negative value is less recognised in the literature. We expect that this is because the continuous relaxation poses fewer problems in these domains than it does for count data.

**Discretization of continuous distributions** A straightforward approach to building a distribution on the integers is to start with a continuous distribution, like a Normal distribution, and to discretize a sample from it. We include two such discretizations below, using a simple rounding operator. In [36] a probabilistic discretization scheme is introduced. This scheme has the benefit over the rounding approach that it preserves expectations.

A slightly different approach is that of creating discrete *analogues* [7]. DALap and DANorm are instances of this approach. In these cases one proceeds by taking key attributes of a continuous distribution, like a maximum entropy property, and finding the integer distribution that shares these properties. In some cases, like the discretized Normal distribution, both approaches yield the same result, but in others, like the discretized Laplace, different solutions may emerge. For a general survey of discretization and discrete analogues, we refer the reader to [12].

## 2.3 Other approaches

Cameron and Johansson [10] introduce a method to modify the density of an arbitrary discrete distribution, with parameters  $\theta$  by a polynomial with parameters  $\mathbf{a}$ . The parameters  $\mathbf{a}$  modify the moments of the base distribution in a predictable way, allowing for over- and underdispersion, and the derivative of the log-likelihood with respect to  $\theta$  and  $\mathbf{a}$  is readily available. We treat this as an extension that may be applied to all integer distributions, including our baselines, and our newly introduced approaches, as well as distributions like the Poisson, which were previously ruled out as viable candidates.

### 3 Methods

In this section, we briefly detail the three existing distributions that satisfy our requirements (discretized Normal, discretized Laplace and Weibull), and then present our three partly novel approaches (Dalap, Danorm and Bitwise).

#### 3.1 Discretized Normal (dnorm)

As noted in the related work, there are various ways to discretize the normal distribution to the integers. For our purposes, the most direct approach is simply to sample from a normal distribution and then round the output to the nearest integer.

More formally, let  $z \sim N(\mu, \sigma)$  with some mean  $\mu$  and standard deviation  $\sigma$ . Let  $r : \mathbb{R} \rightarrow \mathbb{Z}$  be the rounding function which maps the real values  $[n - \frac{1}{2}, n + \frac{1}{2})$  to the integer value  $n$ . Then, we call the distribution on  $r(z)$  the *discretized normal distribution*  $N'$  with parameters  $\mu, \sigma$ .

The probability mass  $N'(n | \mu, \sigma^2)$  can be computed simply from the cumulative distribution function of  $N$ :

$$\begin{aligned} N'(n | \mu, \sigma^2) &= N\left(n - \frac{1}{2} \leq z < n + \frac{1}{2} | \mu, \sigma\right) \\ &= N\left(z < n + \frac{1}{2} | \mu, \sigma\right) - N\left(z < n - \frac{1}{2} | \mu, \sigma\right). \end{aligned}$$

The cumulative distribution can be written in terms of the *error function* as follows.

$$N(z < b | \mu, \sigma) = \frac{1}{2} \left[ 1 + \operatorname{erf}\left(\frac{b - \mu}{\sigma \sqrt{2}} + \epsilon\right) \right]$$

with

$$\operatorname{erf}(x) = \frac{2}{\sqrt{\pi}} \int_0^x e^{-t^2} dt.$$

While the error function has no closed-form solution, various approximations are available which are closed-form.<sup>3</sup> For the backward pass, the derivative

$$\frac{\partial \operatorname{erf}(x)}{\partial x} = \frac{2}{\sqrt{\pi}} e^{-x^2}$$

is easily computed.

---

<sup>3</sup> In our experiments, we use the Pytorch implementation of the error function. This defers to various closed-source systems (depending on backend), for which the approximation used is not usually documented. We use the CUDA backend in all experiments.

### 3.2 Discretized Laplace (dlaplace)

We discretize the Laplace distribution in the same manner as the normal distribution. Let

$$z \sim \text{Laplace}(\mu, b)$$

be a continuous Laplace random variable with location parameter  $\mu$  and scale parameter  $b$ . Its probability density function is given by

$$f(z | \mu, b) = \frac{1}{2b} \exp\left(-\frac{|z - \mu|}{b}\right).$$

Let  $F(z | \mu, b)$  denote the cumulative distribution function of the Laplace distribution:

$$F(z | \mu, b) = \begin{cases} \frac{1}{2} \exp\left(\frac{z - \mu}{b}\right) & \text{if } z < \mu, \\ 1 - \frac{1}{2} \exp\left(-\frac{z - \mu}{b}\right) & \text{if } z \geq \mu. \end{cases}$$

Let  $r : \mathbb{R} \rightarrow \mathbb{Z}$  be defined as in Section 3.1. We then call the distribution of  $r(z)$  the *discretized Laplace distribution*.

The probability mass assigned to an integer  $n$  is computed as

$$P(n | \mu, b) = F\left(n + \frac{1}{2} | \mu, b\right) - F\left(n - \frac{1}{2} | \mu, b\right).$$

Which gives us the following the negative log-likelihood loss:

$$\ell(n | \mu, b) = -\log\left(F\left(n + \frac{1}{2} | \mu, b\right) - F\left(n - \frac{1}{2} | \mu, b\right)\right).$$

For the backward pass, the gradients with respect to  $\mu$  and  $b$  are obtained by differentiating the CDF difference. In particular, the derivatives are given by

$$\frac{\partial \ell}{\partial \mu} = -\frac{1}{b} \left[ \exp\left(\frac{n - \mu}{b}\right) - \exp\left(-\frac{n - \mu}{b}\right) \right],$$

$$\frac{\partial \ell}{\partial b} = -\frac{n - \mu}{b^2} \left[ \exp\left(\frac{n - \mu}{b}\right) + \exp\left(-\frac{n - \mu}{b}\right) \right].$$

### 3.3 Discrete Weibull

The discrete Weibull distribution is an extension of the Weibull distribution [28], specifically designed for discrete, non-negative data, making it well-suited for modeling count data. Unlike the continuous Weibull distribution, the discrete version is characterized by its ability to model varying degrees of dispersion in count data. The probability mass function (PMF) of the discrete Weibull distribution is given by equation 1, where  $\alpha > 0$  is the scale parameter and  $\beta > 0$  is the shape parameter. This difference between consecutive values ensures that each integer count  $x$  has a defined probability.

$$p(X=x) = \exp\left(-\left(\frac{x}{\alpha}\right)^\beta\right) - \exp\left(-\left(\frac{x+1}{\alpha}\right)^\beta\right) \quad (1)$$

Which leads to the following log-probability.

$$\log p(x) = \log\left(1 - \exp\left(\left(\frac{x+1}{\alpha}\right)^\beta - \left(\frac{x}{\alpha}\right)^\beta\right)\right) - \left(\frac{x}{\alpha}\right)^\beta$$

This implementation of the log-probability may lead to unstable gradients. In our implementation, we force the distribution to underflow to negative infinity in case both  $\alpha$  and  $\beta$  are negative infinity.

### 3.4 Discrete analogue of the Laplace distribution (dalap)

In [23], the authors introduce the following discrete analogue of the Laplace distribution:

$$p(n | \mu, \gamma) = \frac{1 - \gamma}{1 + \gamma} \gamma^{|n - \mu|}. \quad (2)$$

Here,  $\gamma$  is a continuous value between 0 and 1, and  $\mu$  and  $n$  are integers. For our purposes, this is not yet a suitable distribution, because  $\mu$  is not continuous.

A simple approach is to assume that  $\mu$  is continuous, and to let  $p(n | \mu, \gamma) \propto \gamma^{|n - \mu|}$ , where  $n - \mu$  is now a continuous value. In order to achieve this, we must change the [partition function](#). First, let

$$f = \mu - \lfloor \mu \rfloor \quad c = \lceil \mu \rceil - \mu \quad \text{dist. to the nearest neighbor of } \mu \text{ }^4$$

So that if  $n \leq \mu$  we have

$$p(n | \mu, \gamma) \propto \begin{cases} \gamma^f \gamma^{\lfloor \mu \rfloor - n} & \text{if } n \geq \mu \\ \gamma^c \gamma^{n - \lceil \mu \rceil} & \text{if } n < \mu \end{cases}$$

Then, for the sum of the unnormalized probability mass  $z$ , we have

$$\begin{aligned} z &= \sum_{i \in \mathbb{Z}} \gamma^{|i - \mu|} = \sum_{i=-\infty}^{\infty} \begin{cases} \gamma^f \gamma^{\lfloor \mu \rfloor - i} & \text{if } i \leq \mu \\ \gamma^c \gamma^{i - \lceil \mu \rceil} & \text{if } i > \mu \end{cases} \\ &= \gamma^f \sum_{i \leq \mu} \gamma^{\lfloor \mu \rfloor - i} + \gamma^c \sum_{i > \mu} \gamma^{i - \lceil \mu \rceil} \\ &= \gamma^f \sum_{j=0}^{\infty} \gamma^j + \gamma^c \sum_{j=0}^{\infty} \gamma^j = (\gamma^c + \gamma^f) \frac{1}{1 - \gamma}. \end{aligned}$$

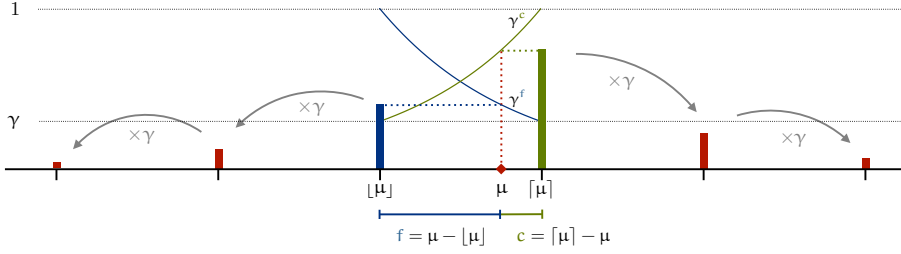


Fig. 1: The principle behind Dalap. The neighbors of  $\mu$  are assigned probability mass between  $\gamma$  and 1 by an exponential function of their distance to  $\mu$ . The rest of the distribution decays geometrically from these two values.

Where the last step uses the well known relation  $\sum_{i=0}^{\infty} \alpha^i = \frac{1}{1-\alpha}$ .

Using  $z^{-1}$  as a partition function, we get

$$p(n | \mu, \gamma) = \frac{1 - \gamma}{\gamma^{\mu - \lfloor \mu \rfloor} + \gamma^{\lceil \mu \rceil - \mu}} \gamma^{|n - \mu|}$$

which reduces to (2) in cases where  $\mu$  takes an integer value, (as the denominator reduces to  $\gamma^0 + \gamma^1 = 1 + \gamma$ ).

Note that even in cases where  $\mu$  is just below or just above an integer value, this definition ensures that a small change in  $\mu$  results in a small change to  $p$ , as required for effective use in gradient descent.

### 3.5 Bounded versions

To constrain the distribution to a subset  $S$  of  $\mathbb{Z}$  we take the unconstrained version of  $p$  and condition on a subset of  $\mathbb{Z}$ . In such cases, the probability mass function is the same as above, except for  $z$ .<sup>5</sup>

We specify two cases: on a one-way bounded interval  $[l, \infty)$ , with  $\mathbb{N}$  as a special case, and on a two-way bounded interval  $[l, u]$ .

For the first, assume first that the interval is  $[0, \infty)$ , from which the general case will follow by change of variables. We have

<sup>4</sup> We define  $\lceil \mu \rceil = \lfloor \mu \rfloor + 1$  to avoid instabilities when  $\mu$  takes an integer value.

<sup>5</sup> By the definition of conditional probability

$$p(n | n \in S) = \frac{p(n)}{\sum_{m \in S} p(m)} = \frac{z^{-1} q(n)}{\sum_m z^{-1} q(m)} = \frac{1}{\sum_m q(m)} q(n)$$

.

$$\begin{aligned}
z_1 &= \sum_{n=0}^{\infty} \begin{cases} \gamma^f \gamma^{\lfloor \mu \rfloor - n} & \text{if } n \leq \lfloor \mu \rfloor \\ \gamma^c \gamma^{n - \lceil \mu \rceil} & \text{if } n > \lceil \mu \rceil \end{cases} \\
&= b_f \sum_{n=0}^{\lfloor \mu \rfloor} \gamma^{\lfloor \mu \rfloor - n} + b_c \sum_{n=\lceil \mu \rceil}^{\infty} \gamma^{n - \lceil \mu \rceil} \\
&= \gamma^f \sum_{i=0}^{\lfloor \mu \rfloor} \gamma^i + \gamma^c \sum_{i=0}^{\infty} \gamma^i \\
&= \gamma^f \frac{1 - \gamma^{\lceil \mu \rceil + 1}}{1 - \gamma} + \gamma^c \frac{1}{1 - \gamma}. \quad \text{note that } \sum_{i=0}^n \alpha^i = \frac{1 - \alpha^{n+1}}{1 - \alpha} \\
&= \frac{\gamma^{\mu - \lfloor \mu \rfloor} (1 - \gamma^{\lceil \mu \rceil + 1})}{1 - \gamma} + \frac{\gamma^{\lceil \mu \rceil - \mu}}{1 - \gamma} \\
&= \frac{\gamma^{\mu - \lfloor \mu \rfloor} - \gamma^{\lceil \mu \rceil + 1 + \mu - \lfloor \mu \rfloor} + \gamma^{\lceil \mu \rceil - \mu}}{1 - \gamma} \\
&= \frac{\gamma^{\mu - \lfloor \mu \rfloor} - \gamma^{\mu + 2} + \gamma^{\lceil \mu \rceil - \mu}}{1 - \gamma}.
\end{aligned}$$

Which gives us

$$p_{\mu, \gamma}(n \mid n \in \mathbb{N}) = \frac{1 - \gamma}{\gamma^{\mu - \lfloor \mu \rfloor} + \gamma^{\lceil \mu \rceil - \mu} - \gamma^{\mu + 2}} \gamma^{|n - \mu|}$$

For other bounds  $[l, \infty)$ , we reparametrize with<sup>6</sup>

$$p_{\mu, \gamma}(n \mid n \geq l) = p_{\mu+l, \gamma}(n+l \mid n \in \mathbb{N}).$$

Finally, for a two-way bounded interval  $[l, u]$ , we have

---

<sup>6</sup> In the rare case of an interval bounded from above, we can reparametrize by first multiplying by  $-1$ .

$$\begin{aligned}
z_2 &= \sum_{n=1}^u \begin{cases} \gamma^f \gamma^{\lfloor \mu \rfloor - n} & \text{if } n \leq \lfloor \mu \rfloor \\ \gamma^c \gamma^{n - \lceil \mu \rceil} & \text{if } n \geq \lceil \mu \rceil \end{cases} \\
&= \gamma^f \sum_{n=1}^{\lfloor \mu \rfloor} \gamma^{\lfloor \mu \rfloor - n} + \gamma^c \sum_{n=\lceil \mu \rceil}^u \gamma^{n - \lceil \mu \rceil} \\
&= \gamma^f \sum_{i=0}^{\lfloor \mu \rfloor - 1} \gamma^i + \gamma^c c \sum_{i=0}^{u - \lceil \mu \rceil} \gamma^i \\
&= \gamma^f \frac{1 - \gamma^{\lfloor \mu \rfloor - l + 1}}{1 - \gamma} + \gamma^c \frac{1 - \gamma^{u - \lceil \mu \rceil + 1}}{1 - \gamma} \\
&= \frac{\gamma^{\mu - \lfloor \mu \rfloor} (1 - \gamma^{\lfloor \mu \rfloor - l + 1})}{1 - \gamma} + \frac{\gamma^{\lceil \mu \rceil - \mu} (1 - \gamma^{u - \lceil \mu \rceil + 1})}{1 - \gamma} \\
&= \frac{\gamma^{\mu - \lfloor \mu \rfloor} - \gamma^{\lfloor \mu \rfloor - l + 1 + \mu - \lfloor \mu \rfloor} + \gamma^{\lceil \mu \rceil - \mu} - \gamma^{u - \lceil \mu \rceil + 1 + \lceil \mu \rceil - \mu}}{1 - \gamma} \\
&= \frac{\gamma^{\mu - \lfloor \mu \rfloor} + \gamma^{\lceil \mu \rceil - \mu} - \gamma^{1 + \mu - l} - \gamma^{1 + u - \mu}}{1 - \gamma}
\end{aligned}$$

Which gives us

$$p_{\mu, \gamma}(n \mid n \in [l, u]) = \frac{1 - \gamma}{\gamma^{\mu - \lfloor \mu \rfloor} + \gamma^{\lceil \mu \rceil - \mu} - \gamma^{1 + \mu - l} - \gamma^{1 + u - \mu}} \gamma^{|n - \mu|}$$

The negative log probabilities for all three versions simplify to

$$-\log p_{\mu, \gamma}(n) = \log z - |\mu - n| \log \gamma$$

where  $z$  depends only on  $\gamma$  in the unbounded case, and on both  $\mu$  and  $\gamma$  in the bounded cases.

Note that this preserves a key property of the non-discrete Laplace distribution that we did not see in the simpler discretized Laplace above: the loss is a linear function of the error  $|\mu - n|$ . That is, to minimize the loss, we minimize the absolute distance between the model prediction  $\mu$  and the target value  $n$ . This loss is then tempered by the amount of uncertainty in a multiplicative factor  $\log \gamma$  and an regularization term  $\log z$ .

In the unbouned case, the regularization term becomes

$$\log z = \log(\gamma^c + \gamma^f) - \log(1 - \gamma).$$

The second term simply promotes low values of  $\gamma$ , forcing the model towards high certainty where possible. This term goes to infinity as  $\gamma \rightarrow 0$ , so its effect

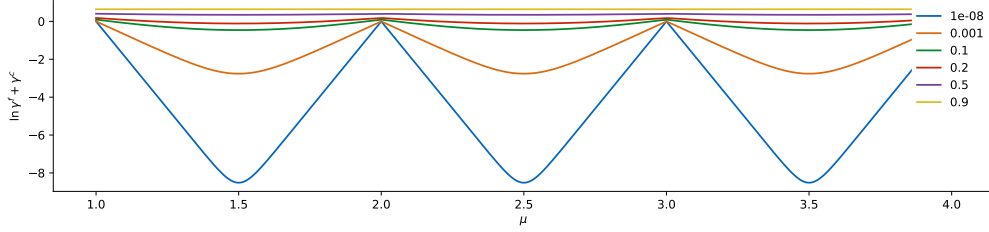


Fig. 2: The value of the penalty term  $\log(\gamma^f + \gamma^c)$  for different values of  $\gamma$ . As the value of  $\gamma$  goes to 0, non-integer values of  $\mu$  are penalized more heavily.

is substantial, but we find similar terms in the negative log probability of the normal and Laplace distributions.<sup>7</sup>

The final regularization term  $\log(\gamma^c + \gamma^f)$  has a natural interpretation too: it forces the output towards integer values, as we become more certain of our prediction. The quantity  $\gamma^c + \gamma^f$  is  $1 + \gamma$  for integer values and  $2\sqrt{\gamma}$  for  $c = f = \frac{1}{2}$ . For  $\gamma \rightarrow 1$ , both values go to 2, and the term behaves as a constant. For  $\gamma \rightarrow 0$ , integer values of  $\mu$  yield  $\log 1$  while non-integer values yield  $\log 0$ . The effect is that as the model converges to lower values of  $\gamma$  (i.e. higher certainty), non-integer values of  $\mu$  are penalized more strongly. In the limit, the model cannot be arbitrarily certain that the true value is a non-integer  $\mu$ , since this term then blows up to  $\infty$ .

### 3.6 Mean and variance.

We will finish up this section with a brief analysis of the mean and variance of the Dalap distribution. For its intended purpose as a neural network loss function, we primarily want to show that the variance can be made sufficiently small around a given expected value, and that this expected value is a simple function of the parameters. In the case of Dalap, we can show that the parameter  $\mu$ , while not equal to the expected value in general, does indeed coincide with the expected value as the variance goes to zero, which we accomplish by letting  $\gamma$  go to zero.

**Proposition 1** *In the unbounded case, the expected value of  $p(n | \mu, \gamma)$  is*

$$\mathcal{E}_{\mu, \gamma} n = \frac{\gamma^f}{\gamma^f + \gamma^c} \left( \lfloor \mu \rfloor - \frac{\gamma}{1 - \gamma} \right) + \frac{\gamma^c}{\gamma^f + \gamma^c} \left( \lceil \mu \rceil + \frac{\gamma}{1 - \gamma} \right)$$

<sup>7</sup> In our implementation we ensure in the activation of  $\gamma$  that its value does not go below a certain  $\epsilon$  to avoid numerical instability.

*Proof.*

$$\begin{aligned}
\mathcal{E}_{\mu, \gamma} n &= \sum_{n \in \mathbb{Z}} p(n | \mu, \gamma) n = \frac{1}{z} \gamma^f \sum_{i=0}^{\infty} \gamma^i (\lfloor \mu \rfloor - i) + \frac{1}{z} \gamma^c \sum_{i=0}^{\infty} \gamma^i (\lceil \mu \rceil + i) \\
&= \gamma^f \lfloor \mu \rfloor \frac{1}{z} \sum_i \gamma^i - \gamma^f \frac{1}{z} \sum_i \gamma^i i + \gamma^c \lceil \mu \rceil \frac{1}{z} \sum_i \gamma^i + \gamma^c \frac{1}{z} \sum_i \gamma^i i \\
&= (\gamma^f \lfloor \mu \rfloor + \gamma^c \lceil \mu \rceil) \frac{1}{z} \frac{1}{1-\gamma} + (\gamma^c - \gamma^f) \frac{1}{z} \frac{\gamma}{(1-\gamma)^2} \quad \text{note } \sum_i \alpha^i i = a/(1-\alpha)^2 \\
&= \frac{1}{z} \frac{\gamma^f \lfloor \mu \rfloor + \gamma^c \lceil \mu \rceil + \gamma^c \frac{\gamma}{1-\gamma} - \gamma^f \frac{\gamma}{1-\gamma}}{1-\gamma} \\
&= \frac{1-\gamma}{1+\gamma} \frac{\gamma^f (\lfloor \mu \rfloor - \frac{\gamma}{1-\gamma}) + \gamma^c (\lceil \mu \rceil + \frac{\gamma}{1-\gamma})}{1-\gamma} \\
&= \frac{\gamma^f \left( \lfloor \mu \rfloor - \frac{\gamma}{1-\gamma} \right) + \gamma^c \left( \lceil \mu \rceil + \frac{\gamma}{1-\gamma} \right)}{\gamma^f + \gamma^c}
\end{aligned}$$

From which the result follows by re-arrangement.  $\square$

This is a weighted sum between a point some distance  $\frac{1}{1-\gamma}$  below  $\lfloor \mu \rfloor$  and another point **the same distance** above  $\lceil \mu \rceil$ . The point  $\lfloor \mu \rfloor - \frac{\gamma}{1-\gamma}$  is the center of mass of the left tail, if  $f = 1$  and likewise for the other term and the right tail. The expectation is a convex combination of both points.

The **weights** are how much  $\gamma^f$  and  $\gamma^c$  respectively claim of the sum  $\gamma^f + \gamma^c$ . See Figure 3 for an illustration.

To understand the behavior of this function, first set  $\mu$  equal to an integer value. Then,  $f$  and  $c$  go to  $\gamma$  and 1. If we then let  $\gamma$  go to 0, we see that the weights go to 0 and 1 and only one of the terms (corresponding to  $\mu$ ) remains. In this term, the **distance** goes to zero with  $\gamma$  and we are left with the value  $\mu$ .

If  $\mu$  does not take an integer value, and we let  $\gamma$  go to zero, we find

$$\lim_{\gamma \rightarrow 0} \frac{\gamma^f}{\gamma^f + \gamma^c} = \lim_{\gamma \rightarrow 0} \frac{1}{1 + \gamma^{c-f}} = \begin{cases} 1 & \text{if } c > f \\ 1/2 & \text{if } c = f \\ 0 & \text{if } c < f \end{cases} \quad (3)$$

and likewise with  $f$  and  $c$  reversed. This tells us that in the limit, the expectation becomes equal to the nearest integer to  $\mu$  (that is,  $r(\mu)$ ) unless  $\mu$  is precisely between two integers, in which case the expectation is  $\mu$ .

This, again, shows a pleasing inductive bias for integer values: as we move to absolute certainty ( $\gamma \rightarrow 0$ ), the expectation takes integer values (except for a zero-measure set of values of  $\mu$  which leads to half-integers).

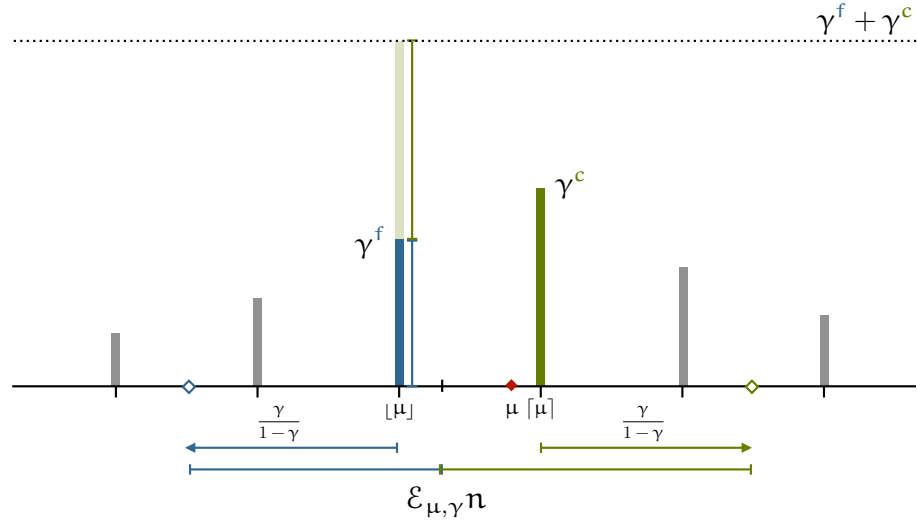


Fig. 3: The expected value of unbounded Dalap. We take two numbers at a distance of  $\frac{\gamma}{1-\gamma}$  below and above  $\lfloor \mu \rfloor$  and  $\lceil \mu \rceil$  respectively. The expected value is a weighted mean of these with weights proportional to  $\gamma^f$  and  $\gamma^c$ .

For the bounded versions of Dalap, we won't compute the full variance, but we will show that the value converges to  $r(\mu)$  as  $\gamma \rightarrow 0$  in the unbounded case, so long as the two neighboring integers are in the support.

**Proposition 2** *If  $\lfloor \mu \rfloor, \lceil \mu \rceil \in S$  then  $\mathcal{E}_{n \sim p(n|n \in S, \mu, \gamma)} n$  goes to  $r(\mu)$  as  $\gamma \rightarrow 0$  unless  $c = f$  in which case it goes to  $\mu$ .*

*Proof.* If  $\mu$  is an integer, the probabilities of  $\mu - 1$  and  $\mu + 1$  are  $\gamma p(\mu)$  and all other integers have lower probability. As  $\gamma \rightarrow 0$ , these go to 0, suggesting that all probability mass is assigned to  $\mu$ , proving the proposition.

For the remainder, assume that  $\mu$  is not an integer. We first write  $\mathcal{E}n = \sum_{n \in S} p(n)n$ .

The probabilities in this sum are of the form  $\gamma^c \gamma^i / (\sum_j \gamma^f \gamma^j + \sum_j \gamma^c \gamma^j)$  for the right tail (with  $c$  replaced by  $f$  in the numerator for the left tail). Writing

$$\lim_{\gamma \rightarrow 0} \frac{\gamma^c \gamma^i}{(\gamma^f + \gamma^c) \sum_j \gamma^j} = \lim_{\gamma \rightarrow 0} \gamma^i \frac{\gamma^c}{\gamma^f + \gamma^c} (1 - \gamma)$$

We note that the factor  $\gamma^i$  causes the probability to go to zero, unless  $i = 0$ . This is only the case for the two neighbors of  $\mu$ , for which the limit goes to  $\frac{\gamma^c}{\gamma^f + \gamma^c}$  for  $\lceil \mu \rceil$  and to  $\frac{\gamma^f}{\gamma^f + \gamma^c}$  for  $\lfloor \mu \rfloor$ .

This gives us

$$\lim_{\gamma \rightarrow 0} \mathcal{E}n = \frac{\gamma^f}{\gamma^f + \gamma^c} \lfloor \mu \rfloor + \frac{\gamma^c}{\gamma^f + \gamma^c} \lceil \mu \rceil.$$

As shown in (3) if  $c \neq f$ , the probabilities go to 0 and 1 leaving only the term corresponding to  $r(\mu)$ . If  $c = f$  the probabilities go to  $\frac{1}{2}$ , leaving us with the midpoint between the two integers which is (in this case) equal to  $\mu$ .  $\square$

**Proposition 3** *The variance of Dalap goes to 0 as  $\gamma \rightarrow 0$ , unless  $c = f$  in which case it goes to  $1/4$ .*

*Proof.* Let  $S \subseteq \mathbb{Z}$  be our support. We write the variance as

$$\mathcal{E}_n n^2 - (\mathcal{E}_n n)^2 = \sum_{n \in S} p(n) n^2 - (\mathcal{E}_n n)^2$$

Assume first that  $c \neq f$ . As  $\gamma \rightarrow 0$ , the second term goes to  $r(\mu)^2$ , following Proposition 2. If  $\mu$  is an integer, we obtain  $n^2 - r(n)^2 = 0$ .

If  $\mu$  is non-integer, only the direct neighbors of  $\mu$  have nonzero probability in the limit (as shown in the proof of Proposition 2). This leaves us with

$$p(\lfloor \mu \rfloor) \lfloor \mu \rfloor^2 + p(\lceil \mu \rceil) \lceil \mu \rceil^2 - \mu^2 = \frac{\gamma^f}{\gamma^f + \gamma^c} \lfloor \mu \rfloor^2 + \frac{\gamma^c}{\gamma^f + \gamma^c} \lceil \mu \rceil^2 - r(\mu)^2$$

As established, the probabilities of the first two terms go to 1 for the term corresponding to  $r(\mu)$ , so that the whole goes quantity goes to 0.

If  $c = f$ , the second term of the expectation goes to  $\mu^2$  and the probabilities go to  $1/2$ , giving us

$$\begin{aligned} \mathcal{E}_n n^2 - (\mathcal{E}_n n)^2 &= \frac{1}{2} \lfloor \mu \rfloor^2 + \frac{1}{2} \lceil \mu \rceil^2 - \mu^2 \\ &= \frac{\lfloor \mu \rfloor^2 + \lceil \mu \rceil^2}{2} - \left( \frac{\lfloor \mu \rfloor + \lceil \mu \rceil}{2} \right)^2 = \frac{1}{4} \end{aligned}$$

Where the last step is derived by substituting  $\lceil \mu \rceil = \lfloor \mu \rfloor + 1$  and multiplying out all squares.  $\square$

This shows that the variance may be made arbitrarily small except for parenthetical values of  $\mu$ , for which the variance is nevertheless a small non-zero value.

### 3.7 Discrete analogue of the normal distribution (danorm)

The main feature of the Laplace distribution is the exponential decay of its tails. Likewise, a defining feature of the normal distribution is the *squared*-exponential decay of its tails. Following this logic, we may ask whether we can take the exponential decay of Dalap and turn it into a squared exponential decay to obtain a discrete analogue for the normal distribution. This gives us the distribution

$$p(n | \mu, \gamma) \propto \gamma^{(n-\mu)^2}.$$

If we set  $\gamma = e^{-\frac{1}{2s}}$ —with  $s$  some alternative dispersion parameter analogous to  $\sigma^2$ —we obtain the more familiar functional form of the normal distribution. Additionally, we can choose our parameters so that this distribution corresponds to the discrete analog of the normal distribution introduced in [24]. Like the normal distribution on the real values, this is the maximum entropy distribution on the integers with given expectation and variance.

Assuming some partition function  $z^{-1}$  and taking the negative log probability, we get

$$-\log p(n | \gamma, \mu) = (n - \mu)^2 \log \gamma - \log z.$$

This shows that, as it does for the normal distribution, our loss becomes a simple tempered version of the squared distance between our location parameter  $\mu$  and the target value  $n$ . The tempering effect of  $\log \gamma$  and  $\log z$  is similar to that in Dalap, due to the similar functional forms.

This suggests that this distribution, which we'll call *Danorm*, is a natural choice for settings where the squared distance is what we are most interested in minimizing, but we still require a discrete distribution on the integers.

The downside of Danorm compared to Dalap is that the partition function has no closed form solution, because unlike the geometric tails of Dalap, there is no elementary closed-form for  $\sum_i \gamma^{(i^2)}$ .

Instead, we rely on the fast decay of the tails to compute  $z$  numerically. For some parameter  $n$  (500 in all experiments), we compute

$$\tilde{z} = \sum_{i \in [\lfloor \mu \rfloor - n, \lceil \mu \rceil + n]} \gamma^{(n-\mu)^2}$$

and substitute this for  $z$ . Additionally we set some maximum value of  $\gamma$  (0.95 in all experiments) to ensure sufficiently fast convergence in the tails.

For bounded versions of Danorm, we then simply set out-of-bounds values to zero in this sum.<sup>8</sup>

This means that the time and memory complexity of computing the loss function increases by a factor of  $2n$  compared to Dalap. In tabular settings, where we compute one probability per instance, this is unlikely to be a bottleneck. However, for something like high-resolution image generation, the overhead may be substantial. In such cases the maximum value of  $\gamma$  should be set low, so that  $n$  can be safely set to low values.

<sup>8</sup> To stabilize the implementation, we actually compute  $\log \tilde{z}$  by computing the log-values of the terms of the sum and summing with the log-sum-exp trick. Out of bound values are set to  $-\infty$ .

**Mean and variance** Due to the lack of a closed form expression for the tails, we cannot provide a similar result to Proposition 1. However, we can show that the expectation converges to  $\mu$  as  $\gamma \rightarrow 0$  and that the variance converges to 0 (with the same exceptions as Dalap). Let  $c$  and  $f$  be defined as they were for Dalap.

**Proposition 4** *If  $\lfloor \mu \rfloor, \lceil \mu \rceil \in S$  then  $\mathcal{E}_{n \sim p(n|n \in S, \mu, \gamma)} n$  goes to  $r(\mu)$  as  $\gamma \rightarrow 0$  unless  $c = f$  in which case it goes to  $\mu$ .*

*Proof.* If  $\mu$  is an integer the result follows by inspection in the same manner as it did for Dalap. If  $\mu$  is non-integer, we first write  $\mathcal{E}n = \sum_{n \in S} p(n)n$ . As with Dalap, we would like to show that only the direct neighbors of  $\mu$  get nonzero probability as  $\gamma \rightarrow 0$ . For the unnormalized probability of some  $n = \lceil \mu \rceil + i$  in the right tail, we have

$$\begin{aligned} \gamma^{(n-\mu)^2} &= \gamma^{(\lceil \mu \rceil + i - \mu)^2} = \gamma^{(c+i)^2} \\ \gamma^{cc+2ci+ci} &= \gamma^{cc} \gamma^{2ci} \gamma^{ii} \end{aligned}$$

and likewise for the left tail.

This gives us for the limit of the corresponding probability

$$\begin{aligned} \lim_{\gamma \rightarrow 0} \frac{\gamma^{cc} \gamma^{2ci} \gamma^{ii}}{\gamma^{ff} \sum_j \gamma^{2fj} \gamma^{jj} + \gamma^{cc} \sum_j \gamma^{2cj} \gamma^{jj}} &= \lim_{\gamma \rightarrow 0} \frac{\gamma^{2ci} \gamma^{ii}}{\sum_j \gamma^{2cj} \gamma^{jj}} \\ &\leq \lim_{\gamma \rightarrow 0} \gamma^{2ci} \gamma^{ii} \frac{\gamma^{cc}}{\gamma^{ff} + \gamma^{cc}} \end{aligned}$$

where the inequality follows from the fact that one term in the sum is equal to 1 (for  $j = 0$ ) and the rest are non-negative. The [first factor](#) in the final result goes to zero except in those cases where  $i = 0$ , which is true for the direct neighbors of  $\mu$ . For those, the first factor goes to 1 and [the second factor](#) remains.

We are left with

$$\mathcal{E}n = \frac{\gamma^{f^2}}{\gamma^{f^2} + \gamma^{c^2}} \lfloor \mu \rfloor + \frac{\gamma^{f^2}}{\gamma^{f^2} + \gamma^{c^2}} \lceil \mu \rceil$$

Rewriting the probabilities as  $\frac{\gamma^{f^2}}{\gamma^{f^2} + \gamma^{c^2}} = \frac{1}{1 + \gamma^{c^2 - f^2}}$  we see that the limit for  $\gamma \rightarrow 0$  is the same as in (3), if  $c > f$  it goes to 0, if  $c = f$  to  $\frac{1}{2}$  and if  $c < f$  to 1, resulting in the same expectation in the limit as we found for Dalap.  $\square$

**Proposition 5** *The variance of Danorm goes to 0 as  $\gamma \rightarrow 0$ , unless  $c = f$  in which case it goes to 1/4.*

*Proof.* We follow the proof for Proposition 3. In the sum, we use the logic from Proposition 4 to isolate only the terms for  $\lfloor \mu \rfloor$  and  $\lceil \mu \rceil$ , resulting in

$$\mathcal{E}_n n^2 - (\mathcal{E}_n n)^2 = \frac{\gamma^{f^2}}{\gamma^{f^2} + \gamma^{c^2}} |\mu|^2 + \frac{\gamma^{c^2}}{\gamma^{f^2} + \gamma^{c^2}} |\bar{\mu}|^2 - r(\mu)^2$$

As established, the limits of these **probabilities** are the same as their equivalents in the proof of Proposition 3, so the same result follows.  $\square$

### 3.8 Bitwise

The *Bitwise* distribution is based on the common practice in neural network modeling of representing integers by their binary representation. While this approach has been used for a long time—for integers or other large discrete output spaces [14, 1]—we believe this is the first *interpretation* of this approach as probability distribution on the integers.

First, let  $\mathbb{B}^k$  represent all bitstrings  $x$  of length  $k$ . We then define the function  $d : \mathbb{B}^k \rightarrow \mathbb{Z}$  as

$$d(x) = (2x_1 - 1)(x_2 2^0 + x_3 2^1 + \dots + x_k 2^{k-2}).$$

That is,  $d(x) = n$  decodes a bitstring to an integer using signed-magnitude representation. We use  $e(n) = x$  for the inverse operation of *encoding* an integer into a bitstring.

Next, we define a parameter vector  $\pi$  with  $k$  real-valued elements  $\pi_i \in [0, 1]$ . We define our distribution on  $\mathbb{Z}$  first from a sampling perspective. For a distribution with parameters  $\pi$  we sample from the corresponding Bitwise distribution, by treating each  $\pi_i$  as a Bernoulli distribution over the values 0 and 1. Sampling from each independently yields a bitstring  $x$ , which we decode as  $d(x) = n$  to obtain the integer  $n$ .

The corresponding probability mass function  $q(n | \pi)$ , by independence is defined simply as

$$\begin{aligned} q(n | \pi) &= \prod_{i=1}^k \text{Bern}(x_i | \pi_i) && \text{with } x = b'(n) \\ &= \prod_i \pi_i^{x_i} (1 - \pi_i)^{1-x_i}. \end{aligned}$$

We must, however, make one exception for  $n = 0$ , which has two possible encodings under  $b$ —one for  $-0$  and one for  $+0$ . To keep our notation simple, we assume that  $q$  is supported by the set of integers with a signed zero. We can then define a distribution on  $\mathbb{Z}$  as

$$p(n | \pi) = \begin{cases} q(+0) + q(-0) & \text{if } n = 0 \\ q(n) & \text{otherwise.} \end{cases}$$

In practice, we always encode 0 as +0. This means that a small amount of probability mass is always expended on unseen events.<sup>9</sup>

**Nonnegative support** Bitwise always has a bounded support of  $[-2^{k-1} + 1, 2^{k-1} - 1]$ . For a version only supported on  $[0, 1, 2, \dots]$ , we remove the sign from the representation, using

$$d(x) = x_1 2^0 + x_2 2^1 + \dots + x_k 2^{k-1}.$$

resulting in a support of  $[0, 2^k - 1]$ . We refer to the first version of Bitwise as *unbounded* and the second as *nonnegative*.

While a support on all of  $\mathbb{Z}$  or  $\mathbb{N}$  is impossible, the size of the support grows exponentially in  $k$ , which means that we can usually set  $k$  large enough to deal with any integers  $n$  we are likely to encounter. We therefore consider bitwise unbounded for practical purposes.<sup>10</sup>

For a two-way bounded version of Bitwise, we can simply choose the smallest interval that takes the form  $[-2^{k-1} + 1, 2^{k-1} - 1]$  or  $[0, 2^k - 1]$  which covers the required interval. Unlike Dalap and Danorm, Bitwise does not allow the support to perfectly coincide with all possible bounds.

**Mean and variance** As with Dalap, we show a brief analysis of the mean and variance, to show that the mean is easily predictable from the parameters and that the variance can be made arbitrarily small. Let  $\text{round}(x)$  be the function that rounds each element of the vector  $x$  to its nearest integer.

*notation* Let  $\pi_i^* = 1 - \pi_i$  and  $\pi_i^x = \begin{cases} \pi_i & \text{if } x_i = 1 \\ \pi_i^* & \text{if } x_i = 0 \end{cases}$  and let  $\pi^x = \pi_1^x \times \dots \times \pi_k^x$ . Let  $\pi_{a:b}$  represent the subvector of  $\pi$  from  $a$  to  $b$  inclusive. If  $a$  or  $b$  is omitted the subvector is taken from the start or end of  $\pi$  respectively.

**Proposition 6** *The mean of a nonnegative Bitwise distribution with parameters  $\pi$  is*

$$\pi_1 2^0 + \dots + \pi_k 2^{k-1}.$$

---

<sup>9</sup> This could be avoided by using a two's complement encoding instead. However, for the upstream model we expect that sign-magnitude representation offers a better separation of concerns, with the magnitude bits representing a magnitude in the same way for both negative and positive integers.

<sup>10</sup> Note that in settings where this is not the case, we would already be unable to represent our data in computer memory using standard integer representations.

*Proof.* We proceed by induction. For the base case where  $k = 1$ , the expected value is  $\pi_1 1 + \pi_1^* 0 = \pi_1 2^0$ . For the inductive case:

$$\begin{aligned}
\mathcal{E}_{n \sim p(x|\pi)} n &= \sum_{n \in (-\infty, \infty)} p(n | \pi) n = \sum_{x \in \mathbb{B}^k} \pi^x d(x) \\
&= \sum_x \pi^x (x_1 2^0 + \dots + x_k 2^{k-1}) = \sum_{x,i} \pi^x x_i 2^{i-1} \\
&= \sum_{i,x \in \mathbb{B}_k^k} \pi^x x_i 2^{i-1} + \sum_{i,x \in \mathbb{B}_{-k}^k} \pi^x x_i 2^{i-1} \\
&= \sum_{i,x \in \mathbb{B}_k^k} \pi^x x_i 2^{i-1} + \sum_{i,x \in \mathbb{B}_{-k}^k} \pi^x x_i 2^{i-1} \\
&= \pi_k \cdot 1 \cdot 2^{k-1} + \pi_1 \sum_{i \in [2,k], x \in \mathbb{B}^{k-1}} \pi_{:k-1}^x x_i 2^{i-1} \\
&\quad + \pi_k^* \cdot 0 \cdot 2^{k-1} + \pi_k^* \sum_{i \in [1,k-1], x \in \mathbb{B}^{k-1}} \pi_{:k-1}^x x_i 2^{i-1} \\
&= \pi_k 2^{k-1} + (\pi_k + \pi_k^*) \sum_{i \in [1,k-1], x \in \mathbb{B}^{k-1}} \pi_{:k-1}^x x_i 2^{i-1} \quad \text{note } \pi_k + \pi_k^* = 1 \\
&= \pi_k 2^{k-1} + \mathcal{E}_{n \sim p(x|\pi_{:k-1})} n.
\end{aligned}$$

By the inductive hypothesis,  $\mathcal{E}_{n \sim p(x|\pi_{:k-1})} n$  is equal to the required remainder of the sum.  $\square$

Note two useful edge cases. In the case that all  $\pi_i = \frac{1}{2}$  we obtain a uniform distribution over  $\mathbb{B}^k$  and thus over  $[0, 2^k - 1]$ . In the case that  $\pi = x$  we obtain a deterministic distribution, where  $p(d(x)) = 1$ .

We next analyze the unbounded case. For ease of notation, we indicate the parameter for the sign bit with  $\pi_{pos}$  and include only the remaining parameters in the vector  $\pi$  (and likewise for  $x$ ). Let  $k$  be the length of  $\pi$  thus defined.

**Proposition 7** *For an unbounded Bitwise distribution with parameters  $\pi_{pos}, \pi$ , the expected value is*

$$(\pi_{pos} - \pi_{pos}^*)(\pi_1 2^0 + \dots + \pi_k 2^{k-1}).$$

*Proof.*

$$\begin{aligned}
\mathcal{E}_{n \sim p(x|\pi)} n &= \sum_{n \in (-\infty, \infty)} p(n | \pi) n = \sum_{x \in \mathbb{B}^k} \pi_{\text{pos}}^x \pi^x d(x) \\
&= \sum_x \pi_{\text{pos}}^x \pi^x (2x_{\text{pos}} - 1)(x_1 2^0 + \dots + x_k 2^{k-1}) \\
&= \sum_x \pi_{\text{pos}} \pi^x (2x_{\text{pos}} - 1) \sum_i x_i 2^{i-1} \\
&= \pi_{\text{pos}} \cdot 1 \cdot \sum_{i, x \in \mathbb{B}^k} \pi^x x_i 2^{i-1} + \pi_{\text{pos}}^* \cdot -1 \cdot \sum_{i, x \in \mathbb{B}^k} \pi^x x_i 2^{i-1} \\
&= (\pi_{\text{pos}} - \pi_{\text{pos}}^*) \sum_{i, x} \pi^x x_i 2^{i-1} = (\pi_{\text{pos}} - \pi_{\text{pos}}^*) \mathcal{E}_{n \sim p(x|\pi, n \geq 0)} n
\end{aligned}$$

Substituting the result from Proposition 6 completes the proof.  $\square$

Next, we show that the variance has a predictable form, which can be made arbitrarily small around an arbitrary value in the support.

**Proposition 8** *The variance of both the unbounded and the non-negative Bitwise distribution goes to 0 as  $\pi \rightarrow x$ .*

*Proof.* We write the variance as  $\mathcal{E}(n - \hat{n})^2$  with  $\hat{n}$  the mean. This gives us for the **nonnegative** distribution

$$\begin{aligned}
\mathcal{E}(n - \hat{n})^2 &= \sum_{x \in \mathbb{B}^k} \pi^x (d(x) - \hat{n}) \\
&= \sum_{x \in \mathbb{B}^k} \pi^x (x_1 2^0 + \dots + x_k 2^{k-1} - \pi_1 2^0 - \dots - \pi_k 2^{k-1})^2 \\
&= \sum_{x \in \mathbb{B}^k} \pi^x ((x_1 - \pi_1) 2^0 + \dots + (x_k - \pi_k) 2^{k-1})^2.
\end{aligned}$$

As  $\pi \rightarrow \bar{x}$  the value  $\pi^x$  goes to 0 for any  $x \neq \bar{x}$  to 1 for  $x = \bar{x}$ , causing all terms but the one corresponding to  $\bar{x}$  to vanish. In that remaining term, the factors  $x_i - \pi_i$  go to zero, since  $\pi_i \rightarrow x_i$ , causing this final term also to vanish, resulting in a variance of 0.

For the **unbounded** distribution, we have

$$\begin{aligned}
\mathcal{E}(n - \hat{n})^2 &= \sum_{x_{\text{pos}} \in \mathbb{B}, x \in \mathbb{B}^k} \pi_{\text{pos}} \pi^x (d(x_{\text{pos}}x) - \hat{n}) \\
&= \sum_{x_{\text{pos}}, x} \pi_{\text{pos}} \pi^x (2x_{\text{pos}} - 1)(x_1 2^0 + \dots + x_k 2^{k-1}) - (\pi_{\text{pos}} - \pi_{\text{pos}}^*) (\pi_1 2^0 + \dots + \pi_k 2^{k-1})^2 \\
&= \pi_{\text{pos}} \sum_x \pi^x (\text{1} \cdot (x_1 2^0 + \dots + x_k 2^{k-1}) - (\pi_{\text{pos}} - \pi_{\text{pos}}^*) (\pi_1 2^0 + \dots + \pi_k 2^{k-1})^2 \\
&\quad + \pi_{\text{pos}}^* \sum_x \pi^x (-\text{1} \cdot (x_1 2^0 + \dots + x_k 2^{k-1}) - (\pi_{\text{pos}} - \pi_{\text{pos}}^*) (\pi_1 2^0 + \dots + \pi_k 2^{k-1})^2) \\
&= \pi_{\text{pos}} \sum_x \pi^x ((x_1 - (\pi_{\text{pos}} - \pi_{\text{pos}}^*) \pi_1) 2^0 + \dots + (x_k - (\pi_{\text{pos}} - \pi_{\text{pos}}^*) \pi_k) 2^{k-1})^2 \\
&\quad + \pi_{\text{pos}}^* \sum_x \pi^x ((-x_1 - (\pi_{\text{pos}} - \pi_{\text{pos}}^*) \pi_1) 2^0 + \dots + (-x_k - (\pi_{\text{pos}} - \pi_{\text{pos}}^*) \pi_k) 2^{k-1})^2
\end{aligned}$$

As  $\pi \rightarrow x$ , we first check whether  $x_{\text{pos}} = 1$ . If so, then the second term vanishes. In the first term, each factor  $x_i - (\pi_{\text{pos}} - \pi_{\text{pos}}^*) \pi_i$  reduces to  $x_i - \pi_i \rightarrow 0$ , making the total sum zero. If  $x_{\text{pos}} = 0$ , the first term vanishes, and in the second term, each factor  $-x_i - (\pi_{\text{pos}} - \pi_{\text{pos}}^*) \pi_i$  reduces to  $-x_i + \pi_i \rightarrow 0$ , and the total sum again goes to 0.  $\square$

## 4 Experiments

We conduct a series of experiments to evaluate the effectiveness of the different distribution functions in modeling integer-valued labels. We use tabular data, sequential time-series data, and image data to provide a comprehensive evaluation. The choice of datasets, including Bicycles, Upvotes, Migration, MAESTRO, MNIST, FashionMNIST and CIFAR10, ensures that the models are tested on the bounded unbounded and one-way bounded methods.

In all experiments, we aim to answer two main questions:

1. Assuming a discrete distribution on the labels is required, which of the five candidates performs best in terms of negative log-loss?
2. Assuming a continuous relaxation is also an option, do any of the five candidates outperform such a relaxation in terms of RMSE?

Each experiment is executed with a sweep over the learning rates:  $3.4 \cdot 10^{-3}, 1 \cdot 10^{-3}, 3.4 \cdot 10^{-4}, 1 \cdot 10^{-4}, 3.4 \cdot 10^{-5}, 1 \cdot 10^{-5}$ . As well as testing various mixture models. We test and compare mixtures of  $k = \{1, 2, 4, 8\}$  where a  $k = 1$  is the standard unmixed distribution (without an extra weight output). Based on the compression loss of the validation set, the results for the test set are reported. All experiments are run with seed 42.

### 4.1 Tabular Regression

We use the following datasets

The **Bicycles** dataset [17] focuses on predicting the hourly number of bicycles parked in a designated space within the Capital Bike Sharing System of Washington D.C. initially comprising 12 features, one-hot encoding of nominal features expands the dataset to 58 features. The dataset is divided into a training set (10,948 samples, 63%), a test set (5,214 samples, 30%), and a validation set (1,217 samples, 7%). The target variable exhibits moderate overdispersion with a dispersion index ( $DI = \sigma^2/\mu$ ) of 173.66 and a skewness of 1.28, indicating a right-skewed distribution with variance substantially exceeding the mean.

The **Upvotes** dataset [29] aims to predict the number of upvotes a social media post will receive. It employs a similar train/test/validation split as the Bicycles dataset, with 207,927 training samples, 99,014 test samples, and 23,104 validation samples. The primary goal is to predict upvotes based on the post's tag, number of answers, and the poster's reputation. One-hot encoding of the tag type (the only nominal feature) and standard scaling of other features results in a total of 12 features. This dataset displays extreme overdispersion ( $DI = 38,238.31$ ) with heavy tails (excess kurtosis = 8,919.66) and severe right-skewness (74.25), characteristic of viral social media dynamics where most posts receive few upvotes while a small fraction achieve disproportionately high engagement.

The **Migration** dataset is a culmination of various datasets of the World Bank Group [37]. This dataset has as a target the net migration [3] with different features from the datasets: agricultural development [2], environmental indicators [5], climate change indicators [4] and the financial sector [6]. This leaves 16,565 instances after combining these different datasets, this merged dataset still includes 8,620 instances which are dropped leaving with a complete dataset of 7,945 instances. Furthermore, the country names are factorized and all features except the country name, year and net migration are Standard Scaled. This gives 4,879 train samples, 2,066 test samples and 1,000 validation samples. Unlike the count-based targets of the previous datasets, net migration includes both positive and negative values with a mean close to zero ( $\mu = 1,601.57$ ) and exhibits extreme variance ( $\sigma^2 = 2.96 \times 10^{10}$ ), resulting in heavy tails (excess kurtosis = 50.21) driven by outlier countries with large migration flows.

All three datasets exhibit significant overdispersion, making them suitable benchmarks for evaluating distribution functions capable of capturing varying degrees of dispersion. We use a multi-layer perceptron (MLP) with ReLU activation functions. The first layer has an input size of  $n$ , the second layer a hidden size of 128 and the output layer a size of 2 in the case of the distributions, 1 in the case of the squared error and 32 in the case of Bitwise.

## 4.2 MAESTRO

The **MAESTRO** (V3) dataset [21] consists of 200 hours of MIDI recordings of professional piano players playing challenging pieces of classical music captured on a digital Piano.

MAESTRO contains 13,424,811 training samples, 4,274,905 test samples and 1,437,884 validation samples. MAESTRO is a curated set of classical piano

music with various levels of expressiveness. This dataset is considered the golden standard for testing any generative music models.

We stop short of building a full generative model for MIDI music—leaving that to future work—and focus only on the task of predicting at any moment in time, *the time in ticks for which the next note will be held*, given the sequence of  $n$  MIDI events observed just before.

The MIDI data is encoded in 5 different events: Event (see table 1), Data1 (Pitch), Data2 (Velocity), Instrument, Channel, and Tick. The first five are embedded with an embedding size of 128. The Tick events are encoded using a linear layer where the tick integer is transformed to a binary string (32 bits) concatenated with the log value of the tick. In table 1 an overview of the value ranges can be found.

Table 1: MIDI representation

Event	Data 1	Data 2	Channel	Instrument	MIDI Tick
Note on	0-127	0-127	0-15	0-127	0- $\infty$
Note off	0-127	0-127	0-15	0-127	0- $\infty$
Polytouch	0-127	0-127	0-15	0-127	0- $\infty$
Pitch Bend	0-127	0-127	0-15	0-127	0- $\infty$
Channel Pressure	0-127	0-127	0-15	0-127	0- $\infty$

To make the predictions, we use an LSTM. The model consists of 2 LSTM layers, each with a hidden dimension of 128. The context length is 128 and the model is trained for 100 epochs. Depending on the distribution target (similarly to the MLP) 2 outputs are used for the distributions, 1 output is used for squared error and 16 for Bitwise (since the highest number in the dataset does not exceed 16 bits there is no need to go over 16 bits in the output).

The model is evaluated every 5000 training samples with a subset of 500 validation samples. After training, we evaluate on the full test data.

During training, the loss is calculated over the entire output sequence and the mean is taken over the batch and sequence. During validation and testing the loss is calculated over only the next token in the sequence which are then summed and averaged over the number of instances.

### 4.3 PixelCNN++

Finally, we explore the task of image generation. For each color channel of each pixel, a generative model on images must produce a distribution on the 255 possible values. So far, this has been done with categorical distributions [31] which ignore the ordinal aspect of the data, or various continuous relaxations [27,32].

A notable advancement in this domain is PixelCNN++ [34], which uses discretized logistic mixtures to model pixel values. While this approach improves

image quality and lowers Bits Per Dimension (BPD) compared to the original PixelCNN, it relies on an underlying continuous density function that is subsequently discretized. In this work, we adopt the architectural backbone of PixelCNN++, specifically the use of padding and shifting over masked kernels, as well as the use of coefficients to maintain RGB ordinality. With this architecture we adopt several distribution functions to compare against the discretized logistic mixture model.

In [34], the authors bridge the gap between continuous predictions and discrete pixel values by integrating the logistic distribution over bins, effectively rounding the continuous values, as in the discretized normal and Laplace distributions above. As we saw in the tabular data, discrete analogues often work better than discretization. We therefore hypothesize that Dalap improves stability during both training and generation by eliminating the need for discretization or rounding.

To validate this, we compare our functions against the original PixelCNN++ results. We evaluate performance using two metrics: Bits Per Dimension (BPD) to measure compression and log-likelihood quality, and the Fréchet Inception Distance (FID) to assess the perceptual quality of the generated images and their similarity to the input distribution across the domains of reconstruction, seeded sampling and random sampling. Furthermore, we investigate whether our method can achieve superior or equal generative performance (lower FID) and likelihood scores (lower BPD) with fewer parameters, thereby demonstrating the efficiency of modeling integer labels with truly discrete distributions.

We evaluate the generative capabilities of our models in three distinct ways:

1. *Unconditional Generation*: Sampling is performed starting from an empty canvas (initialized to a value of -1).
2. *Image Completion*: The model is seeded with the first 8 rows of a ground-truth image from the dataset, and generates the remaining pixels.
3. *Reconstruction*: The model regenerates images based on full input representations.

We use three common low-resolution datasets: MNIST [26] which contains handwritten digits, FashionMNIST [38] which contains images of items of clothing and CIFAR10 [25], which contains color images of ten diverse classes of objects.

Training follows the hyperparameters described in [34]. We use Exponential Moving Average (EMA), and a learning rate decay of 0.99995, with an initial learning rate of  $10^{-3}$  for CIFAR10 and  $10^{-4}$  of FashionMNIST and MNIST. We evaluate each distribution function using both a single component and a mixture of 10 components. All models are trained for 300 epochs across all datasets.

## 5 Results

### 5.1 Count Data Regression

We evaluate several distribution functions for integer-valued regression on four datasets: Bicycles, Upvotes, Migration, and Maestro. Performance is reported in

Tables 2 and 3 using two metrics: Bits (negative log-likelihood in base 2; lower is better) and RMSE (accuracy of the predicted mean; lower is better).

Dalap performs best across all datasets in bits, except for the bicycles dataset with mixture components, where Danorm achieves the lowest bits (6.66). When examining the RMSE scores, Dalap benefits considerably from multiple mixture components, achieving competitive RMSE performance while maintaining the best bits scores. As we consider bits to be the most valuable metric for evaluating distributional modeling quality—since it directly measures how well the model captures the probability distribution—we suggest Dalap as the preferred alternative for discrete data modeling.

Furthermore, our other distribution function, Bitwise, performs well on highly dispersed or varied datasets in terms of bits, but exhibits significantly increased RMSE scores compared to other distribution functions. This suggests that errors in higher-order bits cause the predicted values to drift substantially, leading to large absolute errors despite reasonable probability assignments.

The Laplace, Dnormal, and Danorm functions perform similarly across most datasets, which is expected given their structural similarities in how the distributions are formulated. All three achieve reasonable performance, with Danorm showing particular strength in the mixture setting for the Bicycles dataset.

Finally, Dweib underperforms across multiple metrics, demonstrating its limitations when dealing with under- or over-dispersed data. Its performance on the Upvotes dataset is particularly poor (143.15 bits), and it fails to converge on the Migration dataset, highlighting its unsuitability for data with extreme dispersion characteristics.

When comparing against the squared error baseline (which uses a continuous relaxation), we observe that the continuous approach achieves the best RMSE in three out of four datasets. This suggests that when RMSE is the primary concern and a discrete distribution is not strictly required, continuous relaxations are most likely to provide the best performance, although exceptions exist. However, when a proper discrete distribution is needed—for example, to compute valid log-probabilities or to combine losses from discrete and continuous predictions—Dalap offers the best balance of bits and RMSE performance.

## 5.2 PixelCNN Pixel Regression

For image modeling tasks, we evaluate the distribution functions on MNIST, FashionMNIST, and CIFAR10 datasets. Results are presented in Tables 4 and 5 for single and mixture models respectively, and Tables 6 and 7 for FID scores.

We exclude Dweib and Danorm from the PixelCNN experiments due to practical limitations. Dweib exhibited numerical instability during preliminary experiments, particularly when modeling the bounded [0, 255] range required for pixel values, leading to frequent convergence failures. Danorm, while theoretically sound, requires computing a numerical approximation of the partition function by summing over a range of integers (as described in Section 3.7). For image generation, this computation must be performed for every pixel in every image in the batch, causing requiring large amounts of memory. In our

Table 2: Test set results bicycles, migration, upvotes and maestro, best in bold

	Bicycles		Upvotes		Migration		MAESTRO	
	Bits	RMSE	Bits	RMSE	Bits	RMSE	Bits	RMSE
Dalap	<b>6.76</b>	128	<b>6.75</b>	<b>118</b>	<b>22.80</b>	168 971	<b>5.08</b>	54
Bitwise	7.98	16 149	6.85	8 104	22.94	$3.3 \times 10^9$	5.16	<b>43</b>
Laplace	6.98	68	7.17	395	66.44	<b>169 328</b>	5.42	48
Dnormal	6.89	<b>67</b>	7.10	578	23.25	169 328	5.59	51
Dweib	7.25	115	143.15	2 179	—	—	5.81	66
Danorm	7.31	142	8.12	1 787	4 942.77	169 358	5.26	49
Squared error	—	<b>47</b>	—	1 082	—	<b>40 397</b>	—	<b>32</b>

Table 3: Test set results for mixture models on bicycles, migration, upvotes and maestro, best in bold.

	Bicycles			Upvotes			Migration			MAESTRO		
	K	Bits	RMSE	K	Bits	RMSE	K	Bits	RMSE	K	Bits	RMSE
Dalap	4	6.83	136	8	<b>6.50</b>	<b>120</b>	8	<b>17.73</b>	<b>0</b>	8	<b>4.85</b>	54
Bitwise	8	7.93	4 852	4	6.89	$2.5 \times 10^6$	8	17.96	$3.3 \times 10^9$	8	5.15	88
Laplace	2	6.79	67	8	6.50	294	2	18.72	18 808	8	4.90	54
Dnormal	2	6.84	<b>66</b>	8	6.52	711	8	19.01	41 321	8	4.94	57
Dweib	8	7.14	111	8	6.51	545	—	—	—	8	4.90	55
Danorm	8	<b>6.66</b>	93	4	6.56	1 021	8	1 908.68	169 329	8	4.85	55

experiments, Danorm required over 90GB of VRAM—exceeding our available hardware capacity—making it impractical for image modeling tasks.

**Bits and RMSE** Dalap demonstrates strong performance across all image datasets. In the non-mixture setting (Table 4), Dalap achieves the best bits per dimension on MNIST (0.61) and FashionMNIST (1.23), and performs competitively on CIFAR10 (3.11 bits per dimension), only marginally behind Laplace (3.09). The small difference of 0.02 bits per dimension on CIFAR10 is negligible in practice, especially considering Dalap’s superior performance on the other datasets.

In the mixture setting (Table 5), Dalap maintains its strong performance with 0.66 bits per dimension on MNIST, matching FashionMNIST performance at 1.23, and achieving the best result on CIFAR10 (3.0206 bits per dimension). When comparing against Dlogistic Dalap outperforms it on CIFAR10 by 0.0027 bits per dimension, and shows comparable performance on MNIST (0.66 vs 0.67). This demonstrates that Dalap can match or exceed the performance of the established discretized continuous distribution while maintaining a truly discrete formulation.

Examining RMSE scores, Dalap consistently achieves the lowest values in both single and mixture settings across all datasets. In the mixture models, Dalap achieves RMSEs of 330.48 (MNIST), 317.12 (FashionMNIST), and 510.64 (CIFAR10). This indicates that Dalap not only models the probability distribution well but also produces accurate point predictions. The combination of low bits per dimension and low RMSE suggests that Dalap effectively balances capturing the full distribution with providing reliable predictions of the expected value.

Bitwise shows significantly worse performance on image data, with bits per dimension more than double that of Dalap in most cases. This is particularly pronounced in the mixture setting, where Bitwise achieves 8.02 bits per dimension on CIFAR10 compared to Dalap’s 3.02. The high RMSE values for Bitwise (e.g., 5051.66 on CIFAR10 mixture models) further confirm that representing pixels bit-by-bit introduces substantial prediction errors, likely due to the cascade effect where errors in high-order bits compound into large absolute errors.

The discretized continuous distributions (Laplace and Dnormal) show reasonable performance but generally fall short of Dalap. Laplace performs well on CIFAR10 in both settings but struggles on MNIST (24.47 bits per dimension in the non-mixture case), suggesting that simple discretization may not capture the distribution effectively for all image types. Dnormal exhibits similar patterns, with particularly poor performance on grayscale images.

Table 4: Test set results for image modeling on MNIST, FashionMNIST and CIFAR10, best in bold.

	MNIST		FashionMNIST		CIFAR10	
	Bits/dim	RMSE	Bits/dim	RMSE	Bits/dim	RMSE
Dalap	<b>0.61</b>	<b>253</b>	<b>1.23</b>	<b>317</b>	3.11	<b>480</b>
Bitwise	1.63	535	3.76	881	5.66	1 534
Laplace	24.47	453	5.84	383	<b>3.09</b>	527
Dnormal	9.10	3 992	7.91	3 711	3.37	530

**Fréchet Inception Distance** In the FID scores of generated samples (Tables 6 and 7), we observe nuanced performance patterns that depend on both the dataset and the specific generation task.

In the non-mixture setting (Table 6), Dalap achieves the best seeded sampling performance on MNIST (16.12) and FashionMNIST (52.08), demonstrating its ability to generate high-quality samples when conditioned on partial input. For CIFAR10, Laplace achieves the best seeded sampling score (45.74), closely followed by Dalap (49.76). For random sampling, Dalap excels on MNIST (33.19), while Laplace performs best on CIFAR10 (115.11). Interestingly, Bitwise achieves the best reconstruction FID scores in the non-mixture setting across

Table 5: Test set results for mixture models with a K of 10 on MNIST, FashionMNIST and CIFAR10, best in bold.

	MNIST		FashionMNIST		CIFAR10	
	Bits/dim	RMSE	Bits/dim	RMSE	Bits/dim	RMSE
Dalap	<b>0.66</b>	<b>330</b>	<b>1.23</b>	<b>317</b>	<b>3.02</b>	<b>511</b>
Bitwise	2.71	6 753	4.98	5 699	8.02	5 052
Laplace	3.43	1 085	2.20	3 539	3.05	515
Dnormal	3.97	1 643	3.09	1 111	3.07	516
Dlogistic	0.67	402	1.37	555	3.02	555

all datasets (65.50, 105.50, 119.5), suggesting that its representation may preserve fine-grained details well during reconstruction despite its poor performance in likelihood modeling.

The mixture setting (Table 7) reveals a different pattern. Dlogistic dominates reconstruction tasks across all datasets, achieving FID scores of 42.00 (MNIST), 37.75 (FashionMNIST), and 26.50 (CIFAR10). This superior reconstruction performance likely stems from the smoothness properties of the underlying continuous distribution, which may better capture the perceptual structure of images. However, for sampling tasks, the performance is more balanced. Dalap achieves the best random sampling scores on MNIST (64.75) and FashionMNIST (171.59), while Dlogistic performs best on CIFAR10 (101.71). For seeded sampling, Dlogistic excels on MNIST (18.80), Dalap on FashionMNIST (62.56), and CIFAR10 shows competitive performance across multiple distributions with Laplace (41.12), Dnormal (42.12), and Dalap (44.73) all achieving similar scores.

These results indicate that the choice of distribution for image generation depends on the specific application requirements. Dlogistic offers superior reconstruction quality, making it preferable for tasks like image compression or autoencoding where faithful reproduction is most important. However, Dalap demonstrates competitive or superior performance for sampling tasks, particularly on grayscale datasets (MNIST, FashionMNIST), while maintaining better likelihood scores (bits per dimension) as shown in Tables 4 and 5. The consistently strong performance of Dalap across both likelihood estimation and generative quality metrics suggests it is a robust choice for pixel-level modeling tasks where both probabilistic modeling and sample quality matter.

Bitwise, despite its competitive reconstruction FID in the non-mixture setting, shows poor performance in mixture models and across all sampling tasks, reinforcing our earlier observation that bit-level errors cascade into perceptually significant artifacts. Dnormal exhibits mixed performance, occasionally achieving competitive scores (e.g., 42.12 for CIFAR10 seeded sampling in a mixture setting) but lacking consistency across tasks and datasets.

Table 6: FID scores on test set for image modeling on MNIST, FashionMNIST and CIFAR10, best in bold.

	MNIST			FashionMNIST			CIFAR10		
	Recon.	Seeded	Random	Recon.	Seeded	Random	Recon.	Seeded	Random
Dalap	230	<b>16</b>	<b>33</b>	236	<b>52</b>	<b>154</b>	308	50	146
Bitwise	<b>66</b>	56	90	<b>106</b>	145	299	<b>120</b>	211	290
Laplace	145	109	107	258	102	226	308	<b>46</b>	<b>115</b>
Dnormal	438	274	354	372	268	381	294	67	146

Table 7: FID scores for mixture models with a K of 10 on test set for image modeling on MNIST, FashionMNIST and CIFAR10, best in bold.

	MNIST			FashionMNIST			CIFAR10		
	Recon.	Seeded	Random	Recon.	Seeded	Random	Recon.	Seeded	Random
Dalap	232	54	<b>65</b>	258	<b>63</b>	<b>172</b>	306	45	126
Bitwise	316	287	372	296	275	397	394	264	407
Laplace	232	155	186	304	207	389	306	41	138
Dnormal	249	180	217	306	146	218	308	42	189
Dlogistic	<b>42</b>	<b>19</b>	90	<b>38</b>	69	200	<b>27</b>	<b>41</b>	<b>102</b>

Overall, these experiments demonstrate that Dalap offers state-of-the-art performance for discrete pixel prediction, matching or exceeding the established discretized logistic mixture approach in likelihood estimation while maintaining competitive generative quality, particularly for sampling tasks. The visual samples in Figures 4, 5 and 6 confirm that the quantitative improvements in bits per dimension translate to perceptually high-quality generated images.

**Generated Samples** To qualitatively assess the generative capabilities of the mixture models, we present visual samples in Figures 4, 5 and 6. These figures show results from the mixture models (K=10) which provide the best results.

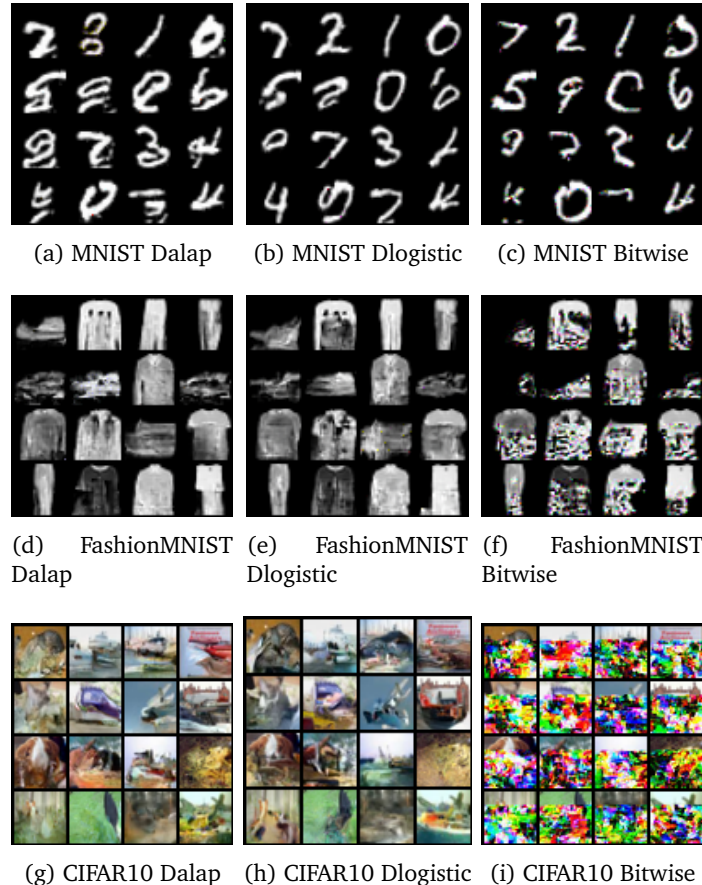


Fig. 4: Seeded sampling results from mixture models ( $K=10$ ). The top portion of each image is provided as conditioning, and the model generates the remainder. Dalap produces high-quality completions across all datasets, with performance comparable to Dlogistic (PixelCNN++) with lower log-likelihood. Bitwise exhibits visible artifacts, particularly on CIFAR10, consistent with its poor quantitative performance.

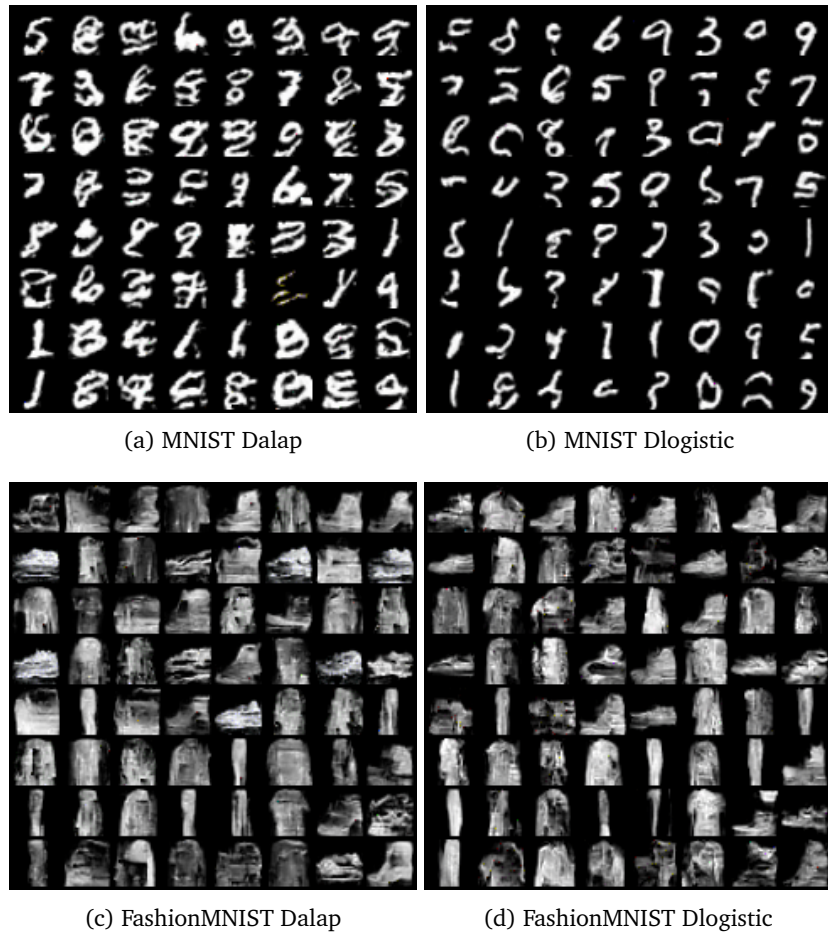


Fig. 5: Random (unconditional) sampling results on MNIST and FashionMNIST from mixture models ( $K=10$ ). All images are generated from scratch without any conditioning.



Fig. 6: Random (unconditional) sampling results on CIFAR10 from mixture models ( $K=10$ ). All images are generated from scratch without any conditioning.

## 6 Conclusion

In this work, we investigate the problem of predicting integer labels from continuous parameters, specifically within the context of neural networks where continuous weights are required for backpropagation. We evaluated several discrete distributions across tabular regression, sequential prediction, and image generation tasks.

Our results demonstrate that modeling integer data with truly discrete distributions can be competitive with continuous relaxations. While continuous relaxations, optimizing for squared error, generally yield the lowest RMSE in tabular settings, they lack the ability to provide valid probability mass functions on the integers. When a discrete distribution is required, for instance to minimize compression loss (bits), we found that the Discrete Analogue of the Laplace distribution (Dalap) and the Bitwise distribution offer the best performance.

Specifically, Dalap consistently achieves state-of-the-art results in terms of negative log-likelihood, matching or exceeding the performance of established methods such as the discretized logistic mixture used in PixelCNN++. It provides a robust balance between minimizing bits and maintaining low RMSE. Furthermore, Dalap offers a more mathematically principled approach to modeling pixel value distributions, which are inherently discrete. In contrast, the discretized logistic relies entirely on continuous computations and only discretizes through rounding at the final prediction stage. The Bitwise distribution proves to be a valuable alternative for high-entropy data; however, it exhibits a high sensitivity to uncertainty in higher-order bits. If the model is uncertain about significant bits, the prediction can deviate substantially from the target, resulting in the high variance and RMSE observed in our experiments.

Ultimately, we conclude that while continuous relaxations remain superior for pure error minimization, Dalap and Bitwise are the preferred choices when a discrete probabilistic model is necessary.

### 6.1 Limitations and Future Work

Our research faced limitations primarily driven by computational constraints. Due to limitations with time and resources, we were unable to perform an exhaustive grid search for the optimal number of mixture components  $K$  for the image modeling experiments. It is possible that fine-tuning this hyperparameter could yield further performance improvements for the mixture models. Since we compare our distribution function to D logistic and use the PixelCNN++ model we decided to use the hyperparameters of their best performing results.

Additionally, while theoretically sound, some distributions proved impractical for high-dimensional tasks. The Discrete Analogue of the Normal distribution (Danorm) requires a numerical approximation of the partition function that scales poorly with input size. In our image generation experiments, Danorm required over 90GB of VRAM, exceeding available hardware capacity and forcing its exclusion from those benchmarks. Similarly, the Discrete Weibull (Dweib) distribution exhibited numerical instability, particularly when modeling bounded

intervals, leading to convergence failures. It may be, however, that with alternative implementations or additional tricks to stabilize learning, the distribution can still be made to work well.

Future work will focus on addressing these stability and efficiency issues. Furthermore, while we demonstrated the efficacy of these distributions on the specific sub-task of predicting note duration in ticks, a natural next step is to integrate Dalap into a full-scale autoregressive generative model for MIDI music, moving beyond conditional scalar prediction to full sequence generation.

**Acknowledgments.** This study was supported by the compute clusters Snellius—under the grant EINF-5362—and DAS6 [8].

**Disclosure of Interests.** The authors have no conflicts of interest to disclose.

## References

1. Nettalk: a parallel network that learns to read aloud. The Johns Hopkins University Electrical Engineering and Computer Science Technical Report (1986)
2. Agriculture & Rural Development. World Bank staff estimates based on the United Nations Population Division’s World Urbanization Prospects: 2018 Revision (2018), Folder IDs SP.RUR.TOTL.ZS, SP.RUR.TOTL.ZG, SP.RUR.TOTL, AG.SRF.TOTL.K2, ISAD(G) Reference Code World Urbanization Prospects: 2018 Revision, [Each Level Label as applicable], World Bank Group Archives, Washington, D.C., United States.
3. Net Migration Data. United Nations Population Division. World Population Prospects: 2022 Revision (2022), Net migration, Folder ID SM.POP.NETM, ISAD(G) Reference Code World Population Prospects: 2022 Revision, [Each Level Label as applicable], World Bank Group Archives, Washington, D.C., United States.
4. Climate Change Indicators. World Bank staff estimates and other relevant data sources (2024), Folder IDs SP.URB.TOTL.IN.ZS, SP.URB.TOTL, SP.POP.TOTL, SP.POP.GROW, ISAD(G) Reference Code Climate Change Statistics and other relevant sources, [Each Level Label as applicable], World Bank Group Archives, Washington, D.C., United States.
5. Environment Indicators. World Bank staff estimates and other relevant data sources (2024), Folder IDs ER.FSH.PROD.MT, ER.FSH.CAPT.MT, ER.FSH.AQUA.MT, ISAD(G) Reference Code International Environmental Statistics and other relevant sources, [Each Level Label as applicable], World Bank Group Archives, Washington, D.C., United States.
6. Financial Sector. World Bank staff estimates and other relevant data sources (2024), Folder IDs SM.POP.NETM, PA.NUS.FCRF, PA.NUS.ATLS, BX.KLT.DINV.CD.WD, ISAD(G) Reference Code International Financial Statistics and other relevant sources, [Each Level Label as applicable], World Bank Group Archives, Washington, D.C., United States.
7. Alzaatreh, A., Lee, C., Famoye, F.: On the discrete analogues of continuous distributions. *Statistical Methodology* **9**(6), 589–603 (2012)
8. Bal, H., Epema, D., de Laat, C., van Nieuwpoort, R., Romein, J., Seinstra, F., Snoek, C., Wijshoff, H.: A medium-scale distributed system for computer science research: Infrastructure for the long term. *Computer* **49**(05), 54–63 (may 2016). <https://doi.org/10.1109/MC.2016.127>

9. Bonat, W.H., Jørgensen, B., Kokonendji, C.C., Hinde, J., Demétrio, C.G.: Extended poisson–tweedie: properties and regression models for count data. *Statistical Modelling* **18**(1), 24–49 (2018)
10. Cameron, A.C., Johansson, P.: Count data regression using series expansions: with applications. *Journal of Applied Econometrics* **12**(3), 203–223 (1997)
11. Cameron, A.C., Trivedi, P.K.: *Regression Analysis of Count Data*, vol. 53. Cambridge University Press (2013)
12. Chakraborty, S.: Generating discrete analogues of continuous probability distributions-a survey of methods and constructions. *Journal of Statistical Distributions and Applications* **2**, 1–30 (2015)
13. Collins, K., Waititu, A., Wanjoya, A.: Discrete weibull and artificial neural network models in modelling over-dispersed count data. *Int J Data Sci Anal* **6**(5), 153–62 (2020)
14. Dietterich, T.G., Bakiri, G.: Solving multiclass learning problems via error-correcting output codes. *J. Artif. Intell. Res.* **2**, 263–286 (1995). <https://doi.org/10.1613/JAIR.105>
15. El-Morshedy, M., Eliwa, M.S., Altun, E.: Discrete burr-hatke distribution with properties, estimation methods and regression model. *IEEE access* **8**, 74359–74370 (2020)
16. Englehardt, J.D., Li, R.: The discrete weibull distribution: An alternative for correlated counts with confirmation for microbial counts in water. *Risk Analysis: An International Journal* **31**(3), 370–381 (2011)
17. Fanaee-T, H.: Bike Sharing. UCI Machine Learning Repository (2013), DOI: <https://doi.org/10.24432/C5W894>
18. Gómez-Déniz, E.: Another generalization of the geometric distribution. *Test* **19**, 399–415 (2010)
19. Gómez-Déniz, E., Calderín-Ojeda, E.: The discrete lindley distribution: properties and applications. *Journal of statistical computation and simulation* **81**(11), 1405–1416 (2011)
20. Grünwald, P.D.: *The minimum description length principle*. MIT press (2007)
21. Hawthorne, C., Stasyuk, A., Roberts, A., Simon, I., Huang, C.Z.A., Dieleman, S., Elsen, E., Engel, J., Eck, D.: Enabling factorized piano music modeling and generation with the MAESTRO dataset. In: International Conference on Learning Representations (2019), <https://openreview.net/forum?id=r1lYRjC9F7>
22. Hilbe, J.M.: *Modeling count data*. Cambridge University Press (2014)
23. Inusah, S., Kozubowski, T.J.: A discrete analogue of the laplace distribution. *Journal of statistical planning and inference* **136**(3), 1090–1102 (2006)
24. Kemp, A.W.: Characterizations of a discrete normal distribution. *Journal of Statistical Planning and Inference* **63**(2), 223–229 (1997)
25. Krizhevsky, A., Hinton, G.: Learning multiple layers of features from tiny images. Tech. rep., University of Toronto (2009)
26. LeCun, Y., Bottou, L., Bengio, Y., Haffner, P.: Gradient-based learning applied to document recognition. *Proceedings of the IEEE* **86**(11), 2278–2324 (1998)
27. Loaiza-Ganem, G., Cunningham, J.P.: The continuous bernoulli: fixing a pervasive error in variational autoencoders (2019), <https://arxiv.org/abs/1907.06845>
28. Nakagawa, T., Osaki, S.: The discrete weibull distribution. *IEEE Transactions on Reliability* **R-24**(5), 300–301 (1975). <https://doi.org/10.1109/TR.1975.5214915>
29. Naseer, U.: Predict the number of upvotes a post will get. <https://www.kaggle.com/datasets/umairnsr87/predict-the-number-of-upvotes-a-post-will-get> (2020), accessed: March 20, 2024
30. Nekoukhous, V., Bidram, H.: The exponentiated discrete weibull distribution. *Sort* **39**, 127–146 (2015)

31. van den Oord, A., Kalchbrenner, N., Vinyals, O., Espeholt, L., Graves, A., Kavukcuoglu, K.: Conditional image generation with pixelcnn decoders (2016), <https://arxiv.org/abs/1606.05328>
32. Ramesh, A., Pavlov, M., Goh, G., Gray, S., Voss, C., Radford, A., Chen, M., Sutskever, I.: Zero-shot text-to-image generation (2021), <https://arxiv.org/abs/2102.12092>
33. Roy, D.: Discrete rayleigh distribution. IEEE transactions on reliability **53**(2), 255–260 (2004)
34. Salimans, T., Karpathy, A., Chen, X., Kingma, D.P.: Pixelcnn++: Improving the pixelcnn with discretized logistic mixture likelihood and other modifications (2017), <https://arxiv.org/abs/1701.05517>
35. Shmueli, G., Minka, T.P., Kadane, J.B., Borle, S., Boatwright, P.: A useful distribution for fitting discrete data: revival of the conway–maxwell–poisson distribution. Journal of the Royal Statistical Society Series C: Applied Statistics **54**(1), 127–142 (2005)
36. Tovissodé, C.F., Honfo, S.H., Doumatè, J.T., Glèlè Kakaï, R.: On the discretization of continuous probability distributions using a probabilistic rounding mechanism. Mathematics **9**(5), 555 (2021)
37. World Bank: World bank website. <https://www.worldbank.org> (2024), accessed: 2024-09-01
38. Xiao, H., Rasul, K., Vollgraf, R.: Fashion-mnist: a novel image dataset for benchmarking machine learning algorithms. arXiv preprint arXiv:1708.07747 (2017)